AIP Advances

RESEARCH ARTICLE | JULY 08 2025

Light-activated self-rectifying resistive switching in $Hf_xTa_yO_z$

Shane M. W. Witsell ; Konner E. K. Holden ; Dustin Z. Austin ; John F. Conley, Jr.

Check for updates

AIP Advances 15, 075014 (2025)
https://doi.org/10.1063/5.0242511

View Online
Export Citation

08 July 2025 19:00:28

AIP Publishing
Special Topics Open for Submissions
Learn More

AIP Publishing

Light-activated self-rectifying resistive switching in $Hf_xTa_yO_z$

Cite as: AIP Advances 15, 075014 (2025); doi: 10.1063/5.0242511
Submitted: 14 April 2025 • Accepted: 1 June 2025 •
Published Online: 8 July 2025

View Online Export Citation CrossMark

Shane M. W. Witsell,[1] Konner E. K. Holden,[2] Dustin Z. Austin,[2] and John F. Conley, Jr.[1,a)]

AFFILIATIONS

[1] School of Electrical Engineering and Computer Science, Oregon State University, Corvallis, Oregon 97331, USA
[2] Lam Research, Tualatin, Oregon 97062, USA

[a)] **Author to whom correspondence should be addressed:** jconley@eecs.oregonstate.edu

ABSTRACT

Light-activated non-volatile bipolar self-rectifying resistive switching was demonstrated in Ag/$Hf_xTa_yO_z$/Si metal/oxide/semiconductor (MOS) devices with $Hf_xTa_yO_z$ deposited via atomic layer deposition. Illumination with visible light enabled the Ag/$Hf_xTa_yO_z$/Si device to be set to the low resistance state (LRS) at a low positive field. The set operation did not occur without illumination. The light-activated set field for $Hf_xTa_yO_z$ devices was much lower than that observed for devices with HfO_2 as the oxide, while in devices with Ta_2O_5, the light-activated switching occurred at low field but suffered from nearly coincident set and threshold fields. The requirement of exceeding a threshold field to reveal the LRS has been referred to as *threshold* switching to distinguish from standard metal oxide resistive random-access memory devices in which the LRS shows an immediate rise in current. A separation of ~0.23 MV/cm between the set and threshold fields in the $Hf_xTa_yO_z$ devices allowed operation as a light-activated non-volatile memory with an LRS/high resistance state ratio of 600:1. No photo-response was seen for metal/insulator/metal devices with a TiN bottom gate, and no light-activated switching was observed in MOS devices with Al top gates, pointing to Ag ion filament formation and dissolution as the primary mechanism for resistive switching.

© 2025 Author(s). All article content, except where otherwise noted, is licensed under a Creative Commons Attribution (CC BY) license (https://creativecommons.org/licenses/by/4.0/). https://doi.org/10.1063/5.0242511

08 July 2025 19:00:28

Resistive switching (RS) is the basis for various non-volatile metal/insulator/metal (MIM) memory technologies, including phase change memory (PCM) and resistive random-access memory (RRAM). The RS process typically involves a rapid, reversible transition between a high-resistance state (HRS) and a low-resistance state (LRS) when critical set (ξ_{SET}) and reset (ξ_{RESET}) switching fields, respectively, are exceeded.[1,2] Switching can be either bipolar or unipolar, where the ξ_{SET} and ξ_{RESET} are of either opposite or the same polarity, respectively.[3] Threshold resistive switching (TRS) is seen in a subset of RS devices characterized by the need to exceed a threshold field (ξ_T) to reveal the LRS, as opposed to standard RS in metal oxide RRAM devices in which the LRS shows an immediate rise in current under bias. TRS has been exploited in selector devices used in memory arrays to prevent sneak currents for applications such as neuromorphic computing.[4–7]

While RS typically relies solely on electrical stimuli, there are reports of light activated/modulated RS in Al_2O_3, SiO_x, GeO, ZnO, ZrO_2,[8–13] $GeSe_{1.5}S_{0.5}$,[14] Si nanocrystals,[15] ZnO nanorods,[16] $ZnWO_4$ nanowires,[17] and graphene oxide based quantum dot-enhanced systems.[18] In addition, light-activated/modulated TRS has been reported in nitrogen-doped graphene oxide quantum dots[19] and VO_2 planar junctions.[20] Light-activated (LA) TRS combines electrical switching with optical illumination, offering the potential to improve the speed, power consumption, and functionality of conventional electrical RS.[13]

HfO_2 and Ta_2O_5 are two of the most widely used materials for RRAM and neuromorphic computing due to excellent switching characteristics and compatibility with CMOS fabrication processes.[21,22] HfO_2 has emerged as a leading candidate due to its high dielectric constant, wide bandgap, and good thermal stability,[23–26] while Ta_2O_5 has shown exceptional endurance of up to 10^{12} switching cycles.[24,27] While there has been an effort to use a nanolaminate of HfO_2 and Ta_2O_5 for standard RS,[28] a ternary $Hf_xTa_yO_z$ oxide approach has yet to be explored for LA-TRS.

In this work, we investigate the LA-TRS properties of $Hf_xTa_yO_z$ deposited via atomic layer deposition (ALD) using metal/oxide/semiconductor (MOS) with Ag and Al top gates and MIM device structures with TiN bottom gates. Switching performance is compared to devices using HfO_2 or Ta_2O_5 alone. The potential mechanisms contributing to LA-TRS are investigated.

© Author(s) 2025

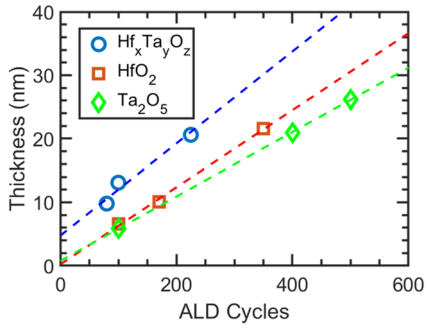

FIG. 1. Plot of film thickness vs ALD cycles for $Hf_xTa_aO_z$ (blue circles), HfO_2 (red squares), and Ta_2O_5 (green diamonds) deposited on Si.

All oxides were deposited via ALD in a PicoSun R150 reactor at 250 °C and ~0.1 Torr. Tetrakis(ethylmethylamido)hafnium (TEMAHf) and H_2O were used for HfO_2 and tantalum(V)ethoxide ($Ta_2(OC_2H_5)_{10}$) and H_2O for Ta_2O_5. Ternary $Hf_xTa_yO_z$ films were deposited via super cycles consisting of a 1:1 ratio of single binary ALD cycles, beginning with HfO_2. Precursors were delivered using N_2 purge separated pulses.

A thickness of 20 nm was targeted for the insulator layer in MOS and MIM devices. Film thickness was measured with a Film Sense FS1000 multi-wavelength ellipsometer. Crystallinity was examined via grazing incidence x-ray diffractometry (GIXRD) measurements using a Rigaku Smart Lab diffractometer.

Oxide insulators were deposited onto either p-type Si substrates (ρ = 0.016 Ω/cm) for MOS devices or TiN/Ti/Si substrates (provided by Onsemi) for MIM devices. Top electrodes were defined by thermally evaporating 50 nm thick, 250 μm diameter Ag or Al circular dots through a shadow mask in a VEECO 7700 thermal evaporator. Contact with the bottom p-Si or TiN electrode was made by gently scratching through the insulator surface on each 2.5 × 2.5 cm^2 coupon with a diamond scribe and soldering on an indium contact (see Fig. S1 in the supplementary material).

Current density vs electric field (J–ξ) measurements were taken using an Agilent 4156C semiconductor parameter analyzer in a probe station at room temperature and in the dark. The applied ξ was swept from −1 to 1 MV/cm and back three times to stabilize device behavior, and the third sweep is shown unless otherwise specified. Illumination was performed using an Osram Halogen 150 W, 21 V lamp. Light was transmitted through an optical cable. The distance between the source and the sample was ~3.8 cm.

Figure 1 is a plot of film thickness vs ALD cycles for HfO_2, Ta_2O_5, and $Hf_xTa_yO_z$. The growth per cycle (GPC) for binary HfO_2 and Ta_2O_5 on Si was determined to be 0.060 nm/cycle and 0.051 nm/cycle, respectively, consistent with previous reports for these precursors.[29,30] $Hf_xTa_yO_z$ growth per 1:1 HfO_2:Ta_2O_5 super-cycle (GPSC), starting with HfO_2, was determined to be 0.073 nm/super-cycle with a nucleation enhancement of 66 cycles. Ta_2O_5 deposited via ALD using these precursors has been recently reported to result in long nucleation delays on HfO_2.[31] However, nucleation enhancement of HfO_2 on Ta_2O_5 in a 10 nm:10 nm ALD nanolaminate was reported using $HfCl_4$ and H_2O.[32] XRD revealed that all films are amorphous or nanocrystalline as-deposited (see Fig. S2 in the supplementary material).

Shown in Fig. 2(a) are plots of J vs ξ for Ag/$Hf_xTa_yO_z$/Si MOS devices in the dark and during subsequent illumination. In the

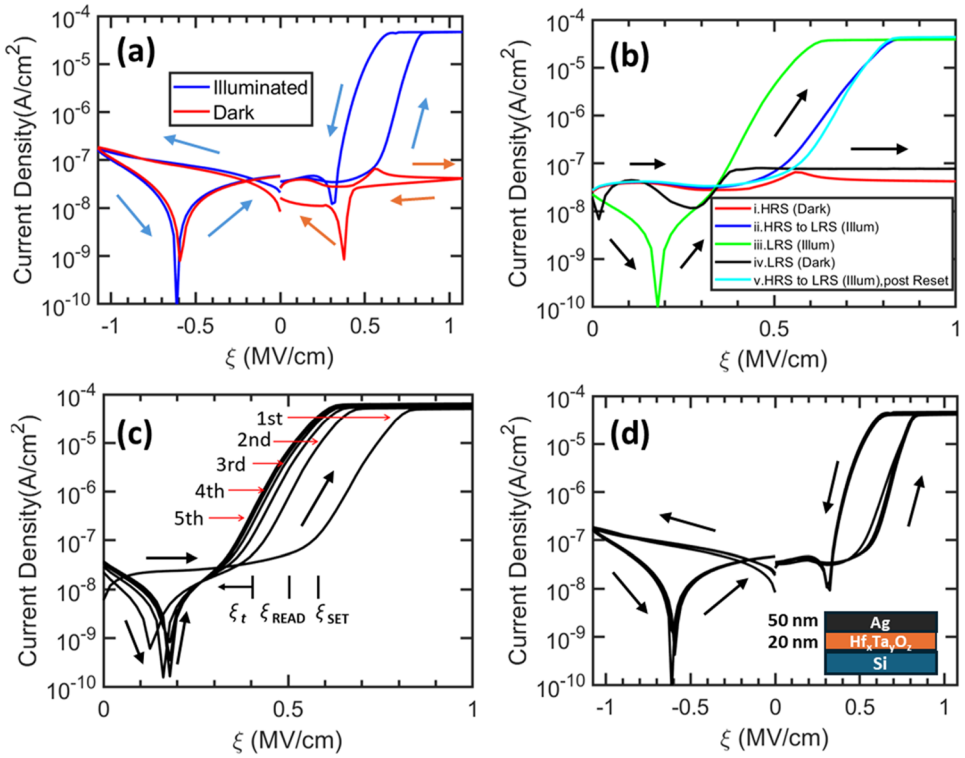

FIG. 2. (a) J–ξ measurements of Ag/$Hf_xTa_yO_z$/Si MOS devices in the dark/prior to illumination (red) and during subsequent illumination (blue). (b) Positive polarity J–ξ for each device operation regime, as described in text. (c) Multiple subsequent positive polarity sweeps under illumination exceeding ξ_{SET}. (d) J–ξ of three sequential full cycle SET and RESET operations while under illumination.

08 July 2025 19:00:28

© Author(s) 2025

dark, the device was in the HRS with a negative differential resistance (NDR) response under positive bias. This behavior has been previously reported in MOS devices and attributed to various mechanisms such as resonant tunneling and filling of interfacial traps.[33,34] The behavior seen in Fig. 2(a) may be caused by filling of a high density of interfacial traps at the oxide/Si interface as the Fermi level rises through the gap under positive gate bias.[35,36] Assuming an amphoteric nature for the traps at the Si/SiO_2 interface and a charge neutral level energy near the middle of the Si bandgap, the current peak corresponds to the position at which the Fermi level was near the middle of the Si bandgap. Another possibility is trap assisted tunneling as the Si valence band aligns and then falls out of alignment with possible oxygen vacancy (V_O) defect levels in the $Hf_xTa_yO_z$.[37]

Illumination produced little change in the negative bias response but a stark shift in the positive bias behavior. At around +0.55 MV/cm, the current density under illumination sharply rose to a saturation level of 4×10^{-5} A/cm^2 (well below the compliance of 2×10^2 A/cm^2), whereas the maximum current in the dark was only 6.5×10^{-8} A/cm^2. The increased current and saturation under illumination are likely a result of the photogeneration of carriers in the Si as compared to the lack of conduction band electrons in the p-type Si substrate in the dark. Increased light intensity (using other visible light sources) results in a higher saturation current, which was previously demonstrated in $Pd/Al_2O_3/SiO_2/Si$ LA-TRS devices.[8] The return sweep from positive to negative ξ indicated that the device had been set to the LRS. The set field, ξ_{SET}, is taken as the field at which current abruptly increased. Although ξ_{SET} happened to correspond roughly to the peak of the current in the dark, they are likely unrelated as the current increase under illumination corresponds to the field at which photogenerated electrons in the Si conduction band begin tunneling with high probability into the conduction band of the $Hf_xTa_yO_z$.

Shown in Fig. 2(b) are sequential positive polarity J–ξ sweeps:

(i) In the dark, prior to illumination, the device is initially in the HRS.

(ii) Next, under illumination, positive sweeping caused the current to increase abruptly and the device was set to the LRS at ξ_{SET} = +0.55 MV/cm. The set occurred with the first positive bias sweep under illumination exceeding ξ_{SET}, without the need for a separate higher field forming sweep as is typically necessary for standard RRAM. Without illumination, the set operation did not occur. On another fresh device from the same test coupon, it was seen that repeated sequential set operations (positive bias sweeps under illumination exceeding ξ_{SET}) resulted in a slight reduction of ξ_T [Fig. 2(c)]. This can be interpreted as "burn-in," indicating a strengthening of the LRS during the initial three sequential set operations.

(iii) With the device now in the LRS, during subsequent positive bias sweeps under illumination, the abrupt increase in current did not take place until a minimum threshold field, ξ_T = 0.32 MV/cm, was exceeded. As $\xi_T < \xi_{SET}$, this indicated that the device remained in the LRS.

(iv) A subsequent sweep in the dark also demonstrated a small current rise at ξ_T with the same slope. Although much smaller than under illumination, this indicated that the device remained in the LRS without continuous illumination. The LRS current is lower in the dark as conduction is limited by lack of available electrons in the p^+ substrate. The device remained in the LRS until application of a *negative* reset field of at least ξ_{RESET} = −0.6 MV/cm, whether the device was under illumination or in the dark.

(v) Following reset, the device remained in the HRS until a subsequent positive bias sweep under simultaneous illumination again exceeded ξ_{SET} = +0.55 MV/cm. The reason that curve (v) is shifted slightly from curve (i) is that curve (i) was the first sweep on the device, normally part of the two-cycle stabilization.

The separation between ξ_T and ξ_{SET} allows the device to be operated as a non-volatile memory. At a read field of ξ_{READ} = +0.5 MV/cm, the LRS/HRS current ratio was 6×10^2 [see Fig. 2(b)]. Shown in Fig. 2(d) are the first three full switching cycles (including the stabilization sweeps) showing repeatability of switching.

Although the set and reset operations were completed under illumination, *continuous* illumination is not required for device operation or for maintenance of the HRS and LRS. A light pulse at the correct voltages could be used to perform the set and read operations.

Shown in Fig. 3 are J–ξ plots for the binary oxide $Ag/HfO_2/Si$ and $Ag/Ta_2O_5/Si$ devices, both in the dark and under illumination, using identical electrical and light exposure conditions as those used for the $Hf_xTa_yO_z$ devices in Fig. 2. The HfO_2 devices [Fig. 3(a)] showed lower leakage than the ternary $Hf_xTa_yO_z$ devices in Fig. 2(b) with a less pronounced NDR regime under positive bias and no switching within the field range of the sweep. To induce switching in HfO_2, ξ_{SET} = +5.4 MV/cm was required, as shown in Fig. 3(b), more than 3 times higher than ξ_{SET} for the $Hf_xTa_yO_z$ devices. The Ta_2O_5 devices [Fig. 3(c)] had substantially higher leakage currents than the HfO_2 devices, comparable to the $Hf_xTa_yO_z$ devices. The Ta_2O_5 devices, however, suffered from nearly coincident ξ_{SET} and ξ_T (both being approximately +0.3 MV/cm), and thus, it was not possible to read the device without a simultaneous set into the LRS. The ternary $Hf_xTa_yO_z$ devices in Fig. 2 thus appeared to combine the low ξ_T of the HfO_2 devices with the low ξ_{SET} of the Ta_2O_5 devices, maintaining the separation of ξ_{SET} and ξ_T and enabling non-volatile memory (NVM) operation at lower power than for HfO_2 devices.

The physical mechanism commonly reported for the bipolar RS behavior of many metal–oxide RRAM devices is the formation (set to LRS) and dissolution (reset to HRS) of conductive filaments (CFs) within the oxide that serve as a conductive bridge between the electrodes. CF formation and dissolution occur via the motion of mobile charged species under bias. Assuming a CF mechanism, two possibilities for the mobile charged species in these devices are (i) Ag^+ ions from the electrode and/or (ii) Vo^+.[38–40] Ag is commonly used as an electrode in electrochemical dissolution based resistive memories.[41] A role for Ag^+ ions is supported by the positive set and negative reset fields, pointing to field-driven movement away from the top electrode through the oxide toward the bottom Si electrode and then back away from the Si, respectively.[42] In this scenario, once ξ_{SET} is reached, the Ag^+ ions assemble to form a continuous CF bridge to the Si electrode. The negative ξ_{RESET} would subsequently dissolve the CF. The requirement of exceeding ξ_T to reestablish the LRS, as opposed to an immediate rise in current, has been interpreted as instability of the CF, meaning that below ξ_T, part of the

08 July 2025 19:00:28

© Author(s) 2025

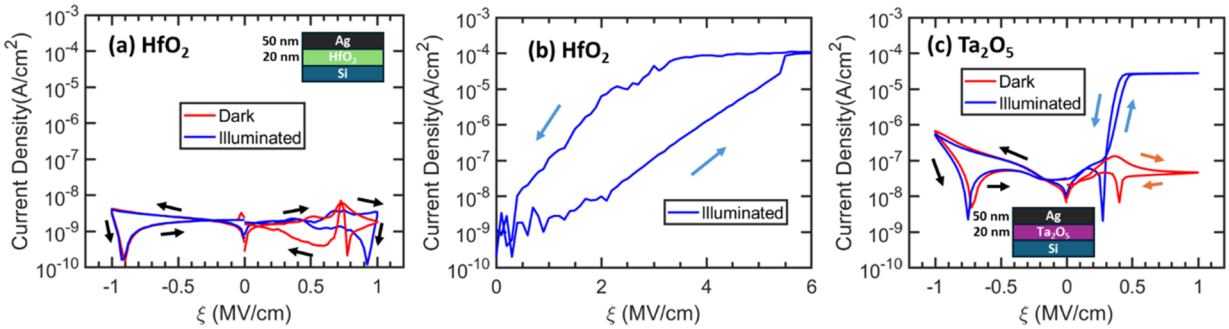

FIG. 3. Plots of J–ξ for (a) HfO_2, (b) HfO_2 with an extended positive bias sweep under illumination, and (c) and Ta_2O_5 MOS devices taken in the dark and under illumination.

CF transforms into disordered ion clusters, breaking the CF without resetting the device so that as the applied field rises above ξ_T (which is below ξ_{SET}), the LRS bridge easily reforms.[4] In this scenario, the decrease in ξ_T with additional sequential SET operations seen in Fig. 2(d) would suggest formation of more robust CF(s). However, the ξ_T requirement here is likely simply due to the Schottky barrier expected between the Ag filament bridge and the p^+ Si substrate.

V_O filament formation has been established as the primary mechanism in many reports of metal oxide RRAM devices.[22,43] For RS devices based on HfO_2 with Ag top electrodes and p-Si bottom electrodes, a mixed Ag and V_O filament has been suggested.[41] It has also been suggested that increased electron injection from the Si under positive gate bias and illumination can assist in Si–O bond breakage, generating additional V_O's at/near the Si/oxide interface.[12,19] V_O's are well known to act as intrinsic donors and/or charge traps in many metal oxides, and thus, the movement of V_O toward and away from the electrode interfaces under bias could modulate the width of the Schottky barrier in the oxide and thus its transmission probability.[17,44–47] Both V_O roles, however, are *inconsistent* with the switching polarities seen here as filament formation would require the V_O^+ to move in the direction opposing the bias field, and if V_O^+ were neutralized by capturing injected electrons, the LRS state would be impaired rather than enhanced.

Another proposed mechanism for LA-TRS is metal nanoparticle photoemission (MNP), in which illumination is postulated to cause internal photoemission from metallic Ag^+ nanoparticles in the oxide, increasing the electric field strength near the oxide/Si interface thus lowering the switching threshold.[13] MNP, however, is not likely present in these devices as the ξ_{RESET} remains the same regardless of whether the device is in the dark or under illumination indicating no change to the negative field under illumination.

To further elucidate the potential roles of Ag^+ and V_O^+ in the LA-TRS devices, electrode dependence was investigated using two additional device structures: (i) Ag/$Hf_xTa_yO_z$/TiN MIM devices to assess the influence of a metallic vs the p-Si bottom electrode and (ii) Al/$Hf_xTa_yO_z$/Si MOS devices to remove the possibility of mobile Ag^+ ions. J–ξ behavior is shown in Fig. 4. The Al/$Hf_xTa_yO_z$/Si MOS device showed response to illumination, while the Ag/$Hf_xTa_yO_z$/TiN MIM device did not. Shown in Fig. 4(a), the positive polarity saturation current of the Al/$Hf_xTa_yO_z$/Si device was much higher under illumination, confirming that the light activation effects seen in the Ag/$Hf_xTa_yO_z$/Si devices (Fig. 2) were primarily due to photogeneration in the p-Si, rather than visible spectrum MNP from Ag^+ ions.[13] However, despite responding to illumination, the Al/$Hf_xTa_yO_z$/Si device did *not* exhibit LA-RS at positive bias, indicating that Ag+ ions must play a major role in RS.

The Ag/$Hf_xTa_yO_z$/TiN MIM device [Fig. 4(b)] also did not show positive bias switching behavior within the field range seen for the Ag/$Hf_xTa_yO_z$/Si devices, indicating that the combination of the Ag electrode and the p-Si substrate was prerequisite for LA-TRS. The Ag/$Hf_xTa_yO_z$/TiN device did show the onset of gradual RS at positive bias, with or without light, pointing to a different mechanism [Fig. 4(c)].

In summary, light-activated bipolar threshold-field resistance switching was demonstrated in Ag/$Hf_xTa_yO_z$/Si MOS devices using a 20 nm-thick $Hf_xTa_yO_z$ deposited via ALD. Under illumination with visible light, Ag/$Hf_xTa_yO_z$/Si devices were set from the initial HRS to the LRS at ξ_{SET} = +0.55 MV/cm. The set operation did not occur in the dark. Subsequent positive polarity sweeps required exceeding a ξ_T = 0.32 MV/cm to access the LRS. RS devices requiring a ξ_T are generally referred to threshold switching devices to distinguish them from typical RRAMs in which the current increase under bias is immediate in the LRS. Devices were reset from the LRS to the HRS at ξ_{RESET} = −0.6 MV/cm regardless of illumination. The field separation of ~0.2 MV/cm between ξ_{SET} and ξ_T allowed the device to be operated as an NVM with an LRS/HRS current ratio of 600:1 at an ξ_{READ} = +0.5 MV/cm. Similar positive polarity light activated switching behavior was observed in HfO_2 devices but required nearly 3× higher applied fields, while the LA switching in Ta_2O_5 devices occurred at low field but suffered from nearly coincident ξ_{SET} and ξ_T, prohibiting use as a NVM. The ternary $Hf_xTa_yO_z$ devices appeared to combine the low ξ_T of the HfO_2 devices with the low ξ_{SET} of the Ta_2O_5 devices, creating the separation of ξ_{SET} and ξ_T to enable NVM operation at lower power than for HfO_2 devices.

For Ag/$Hf_xTa_yO_z$/TiN MIM devices with TiN bottom gates, illumination had no impact on device operation, indicating that photo-generation in the Si was required for LA switching. Al/$Hf_xTa_yO_z$/Si MOS devices, in which Ag was replaced with Al, showed an illumination induced increase in current under positive bias due to photo-generation in the Si. However, these devices showed no switching, pointing to Ag^+ ion filament formation and dissolution as the dominant mechanism for RS.

08 July 2025 19:00:28

© Author(s) 2025

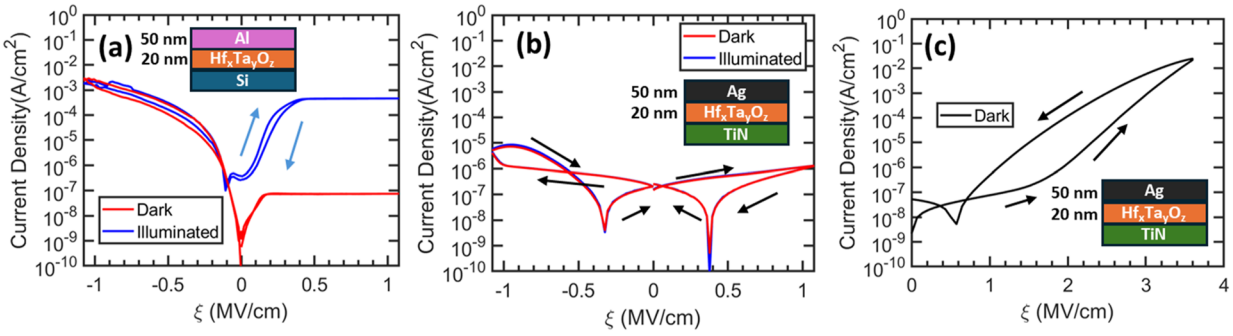

FIG. 4. Plots of J–ξ for (a) Al/$Hf_xTa_yO_z$/Si MOS and (b) Ag/$Hf_xTa_yO_z$/TiN MIM devices taken in the dark and under illumination. (c) Ag/$Hf_xTa_yO_z$/TiN MIM devices with an extended positive bias sweep.

Light-activated self-rectifying $Hf_xTa_yO_z$ based MOS devices show promise for reduced power CMOS compatible NVM. Further enhancements to switching performance might be found in the use of other diffusive top electrodes for improved CF formation, modifications to the ALD process to adjust oxide stoichiometry or engineer interfacial defects and V_O's, use of an entropy stabilized oxide (ESO) phase to potentially enhance ion mobility,[48] and optimizing doping in the Si to modulate the Schottky barrier and potentially improve ξ_T. *In-operando* evaluation of the electron barrier height at the electrode/$Hf_xTa_yO_z$ interfaces via internal photoemission (IPE) spectroscopy would help determine the role of Schottky barriers in TRS.[49,50]

See the supplementary material for plot of XRD scans taken on as-deposited devices demonstrating their amorphous nature.

This work was conducted at the Materials Synthesis and Characterization (MaSC) Center, a National Nanotechnology Coordinated Infrastructure (NNCI) Northwest Nanotechnology Infrastructure (NWNI) user facility at Oregon State University. The authors thank Chris Tasker and Rick Presley of Oregon State University for equipment support. XRD was conducted at the University of Oregon. TiN/Ti/SiO_2/Si substrates were provided by Onsemi. This work was funded in part by an Unlock Ideas gift from Lam Research.

AUTHOR DECLARATIONS

Conflict of Interest

The authors have no conflicts to disclose.

Author Contributions

Shane M. W. Witsell: Conceptualization (equal); Data curation (lead); Formal analysis (equal); Investigation (lead); Methodology (lead); Visualization (lead); Writing – original draft (lead); Writing – review & editing (equal). **Konner E. K. Holden**: Conceptualization (equal); Funding acquisition (supporting); Supervision (supporting); Writing – review & editing (supporting). **Dustin Z. Austin**: Conceptualization (supporting); Funding acquisition (supporting); Supervision (supporting); Writing – review & editing (supporting). **John F. Conley, Jr.**: Conceptualization (equal); Formal analysis (equal); Funding acquisition (lead); Project administration (lead); Resources (lead); Supervision (lead); Visualization (equal); Writing – original draft (equal); Writing – review & editing (lead).

DATA AVAILABILITY

The data that support the findings of this study are available from the corresponding author upon reasonable request.

REFERENCES

[1] M. Le Gallo, A. Athmanathan, D. Krebs, and A. Sebastian, J. Appl. Phys. **119**(2), 025704 (2016).
[2] N. Saxena, R. Raghunathan, and A. Manivannan, Sci. Rep. **11**(1), 6111 (2021).
[3] W. Guan, S. Long, Q. Liu, M. Liu, and W. Wang, IEEE Electron Device Lett. **29**(5), 434–437 (2008).
[4] Y. Choi, J. Shin, S. Moon, and C. Shin, Micromachines **11**, 525 (2020).
[5] I. Zrinski, J. Zavašnik, J. Duchoslav, A. W. Hassel, and A. I. Mardare, J. Nanomater. **12**(22), 3944 (2022).
[6] Y.-J. Huang, S.-C. Chao, D.-H. Lien, C.-Y. Wen, J.-H. He, and S.-C. Lee, Sci. Rep. **6**(1), 23945 (2016).
[7] W. Banerjee, X. Xu, H. Liu, H. Lv, Q. Liu, H. Sun, S. Long, and M. Liu, IEEE Electron Device Lett. **36**, 333 (2015).
[8] M. Ungureanu, R. Zazpe, F. Golmar, P. Stoliar, R. Llopis, F. Casanova, and L. E. Hueso, Adv. Mater. **24**(18), 2496–2500 (2012).
[9] A. Mehonic, T. Gerard, and A. J. Kenyon, Appl. Phys. Lett. **111**(23), 233502 (2017).
[10] V. A. Volodin, G. N. Kamaev, and M. Vergnat, Phys. Status Solidi RRL **14**(7), 2000165 (2020).
[11] S. V. Tikhov, O. N. Gorshkov, M. N. Koryazhkina, I. N. Antonov, and A. P. Kasatkin, Tech. Phys. Lett. **42**(5), 536–538 (2016).
[12] O. Blázquez, J. L. Frieiro, J. López-Vidrier, C. Guillaume, X. Portier, C. Labbé, S. Hernández, and B. Garrido, Appl. Phys. Lett. **115**(26), 261104 (2019).
[13] A. S. Novikov, D. O. Filatov, M. E. Shenina, I. N. Antonov, D. A. Antonov, A. V. Nezhdanov, V. A. Vorontsov, D. A. Pavlov, and O. N. Gorshkov, J. Phys. D: Appl. Phys. **54**(48), 485303 (2021).
[14] R. T. Ananth Kumar, C. Das, P. Chithra Lekha, S. Asokan, C. Sanjeeviraja, and D. Pathinettam Padiyan, J. Alloys Compd. **615**, 629–635 (2014).
[15] J. López-Vidrier, J. L. Frieiro, O. Blázquez, D. Yazicioglu, S. Gutsch, K. E. González-Flores, M. Zacharias, S. Hernández, and B. Garrido, Appl. Phys. Lett. **116**(19), 193503 (2020).
[16] J. Park, S. Lee, and K. Yong, Nanotechnology **23**(38), 385707 (2012).

08 July 2025 19:00:28

© Author(s) 2025

[17]W. X. Zhao, B. Sun, Y. H. Liu, L. J. Wei, H. W. Li, and P. Chen, AIP Adv. **4**(7), 077127 (2014).
[18]G. N. Panin, Chaos, Solitons Fractals **142**, 110523 (2021).
[19]M. Ali, A. Sokolov, M. J. Ko, and C. Choi, J. Alloys Compd. **855**, 157514 (2021).
[20]G. Seo, B.-J. Kim, Y. Wook Lee, and H.-T. Kim, Appl. Phys. Lett. **100**(1), 011908 (2012).
[21]S. Brivio, S. Spiga, and D. Ielmini, Neuromorph. Comput. Eng. **2**(4), 042001 (2022).
[22]J. H. Yoon, Y.-W. Song, W. Ham, J.-M. Park, and J.-Y. Kwon, APL Mater. **11**(9), 090701 (2023).
[23]Z. Wu, X. Zhao, Y. Yang, W. Wang, X. Zhang, R. Wang, R. Cao, Q. Liu, and W. Banerjee, Nanoscale Adv. **1**(9), 3753–3760 (2019).
[24]M. Hellenbrand and J. MacManus-Driscoll, Nano Convergence **10**, 44 (2023).
[25]D. Walczyk, C. Walczyk, T. Schroeder, T. Bertaud, M. Sowińska, M. Lukosius, M. Fraschke, B. Tillack, and C. Wenger, Microelectron. Eng. **88**(7), 1133–1135 (2011).
[26]C.-F. Liu, X.-G. Tang, L.-Q. Wang, H. Tang, Y.-P. Jiang, Q.-X. Liu, W.-H. Li, and Z.-H. Tang, Nanomaterials **9**(8), 1124 (2019).
[27]A. R. Patil, T. D. Dongale, R. K. Kamat, and K. Y. Rajpure, Mater. Today Commun. **34**, 105356 (2023).
[28]S. Kim, Y. Abbas, Y.-R. Jeon, A. S. Sokolov, B. Ku, and C. Choi, Nanotechnology **29**(41), 415204 (2018).
[29]Y. Yokoyama, S. Zhu, and A. Nakajima, Jpn. J. Appl. Phys. **45**, 7091–7093 (2006).
[30]T. Henke, M. Knaut, M. Geidel, F. Winkler, M. Albert, and J. W. Bartha, Thin Solid Films **627**, 94–105 (2017).
[31]Y. Li, Y. Lan, K. Cao, J. Zhang, Y. Wen, B. Shan, and R. Chen, Chem. Mater. **34**(20), 9013–9022 (2022).
[32]K. Kukli, J. Ihanus, M. Ritala, and M. Leskela, Appl. Phys. Lett. **68**(26), 3737–3739 (1996).
[33]R. Pant, N. Patel, K. K. Nanda, and S. B. Krupanidhi, J. Appl. Phys. **122**(12), 125303 (2017).
[34]M. Dragoman and D. Dragoman, Solid-State Electron. **197**, 108464 (2022).
[35]H. Çetin and E. Ayyıldız, Appl. Surf. Sci. **253**, 5961–5966 (2007).
[36]M. N. Getz, M. Povoli, and E. Monakhov, J. Appl. Phys. **129**(20), 205701 (2021).
[37]G. Woo, T. Kim, and H. Yoo, Adv. Electr. Mater. **9**(2), 2201015 (2023).
[38]F. Zahoor, F. A. Hussin, U. B. Isyaku, S. Gupta, F. A. Khanday, A. Chattopadhyay, and H. Abbas, Discover Nano **18**(1), 36 (2023).
[39]M. N. Kozicki and H. J. Barnaby, Semicond. Sci. Technol. **31**(11), 113001 (2016).
[40]J. Ryu, K. Park, D. P. Sahu, and T.-S. Yoon, ACS Appl. Mater. Interfaces **16**(20), 26450–26459 (2024).
[41]S. Saylan, H. M. Aldosari, K. Humood, M. Abi Jaoude, F. Ravaux, and B. Mohammad, Sci. Rep. **10**, 19541 (2020).
[42]I. Valov, R. Waser, J. R. Jameson, and M. N. Kozicki, Nanotechnology **22**(28), 289502 (2011).
[43]K. Park and J.-S. Lee, RSC Adv. **6**(26), 21736–21741 (2016).
[44]P. M. Lenahan and J. F. Conley, Jr., IEEE Trans. Device Mater. Reliab. **5**(1), 90–102 (2005).
[45]N. Alimardani and J. F. Conley, Jr., Appl. Phys. Lett. **105**(8), 082902 (2014).
[46]E. Mikheev, B. D. Hoskins, D. B. Strukov, and S. Stemmer, Nat. Commun. **5**(1), 3990 (2014).
[47]J. S. Lee, S. Lee, and T. W. Noh, Appl. Phys. Rev. **2**(3), 031303 (2015).
[48]D. Bérardan, S. Franger, A. K. Meena, and N. Dragoe, J. Mater. Chem. A **4**(24), 9536–9541 (2016).
[49]J. Haglund, T. Mimura, J. F. Ihlefeld, and J. F. Conley, Jr., ACS Appl. Electron. Mater. **6**(5), 3249–3256 (2024).
[50]M. A. Jenkins, K. E. K. Holden, S. W. Smith, M. T. Brumbach, M. D. Henry, C. Weiland, J. C. Woicik, S. T. Jaszewski, J. F. Ihlefeld, and J. F. Conley, Jr., ACS Appl. Mater. Interfaces **13**(12), 14634–14643 (2021).

08 July 2025 19:00:28

© Author(s) 2025